Optimal frequency-response sensitivity of compressible flow over roughness elements

Miguel Fosas de Pando[1] **and Peter J Schmid**[2]

[1] Department of Mechanical Engineering and Industrial Design, University of Cádiz, 11001 Cádiz, Spain
[2] Department of Mathematics, Imperial College London, London, SW7 2AZ, United Kingdom

E-mail: `miguel.fosas@uca.es`

Abstract. Compressible flow over a flat plate with two localized and well-separated roughness elements is analyzed by global frequency-response analysis. This analysis reveals a sustained feedback loop consisting of a convectively unstable shear-layer instability, triggered at the upstream roughness, and an upstream-propagating acoustic wave, originating at the downstream roughness and regenerating the shear-layer instability at the upstream protrusion. A typical multi-peaked frequency response is recovered from the numerical simulations. In addition, the optimal forcing and response clearly extract the components of this feedback loop and isolate flow regions of pronounced sensitivity and amplification. An efficient parametric-sensitivity framework is introduced and applied to the reference case which shows that first-order increases in Reynolds number and roughness height act destabilizing on the flow, while changes in Mach number or roughness separation cause corresponding shifts in the peak-frequencies. This information is gained with negligible effort beyond the reference case and can easily be applied to more complex flows.

1. Introduction

The behavior of many fluid flows is often dominated by an intricate interplay between advective, diffusive and feedback processes. If more complex flow situations are considered with, e.g., reactive, temperature-dependent, surface-driven, particle-laden, radiative or non-Newtonian subprocesses, an even more complicated network of interactions needs to be analyzed to determine the underlying physics that manifests itself in the rise to coherent structures in the form of instabilities or the response to environmental forcings. Particularly when dominant feedback elements are present in the flow, a global analysis is required. For globally stable systems that act as selective amplifiers of environmental disturbances, a study of the frequency response to harmonic, external forcing is appropriate and furnishes insight into prevalent scale-selection and feedback mechanisms in the flow. Mathematically, this type of analysis establishes the transfer function of the flow, including a hierarchy of input and output structures corresponding to a given frequency. The latter information identifies regions of the flow that are particularly sensitive to harmonic forcing (input) and display maximal effects of periodic driving (output). A frequency-response analysis (also known as resolvent or input-output analysis) is especially effective when multiple physical processes compete in establishing observed amplification mechanisms; in this case, judiciously chosen input and/or output weights can help explore and quantify a multitude of energy paths through a network of possible interactions.
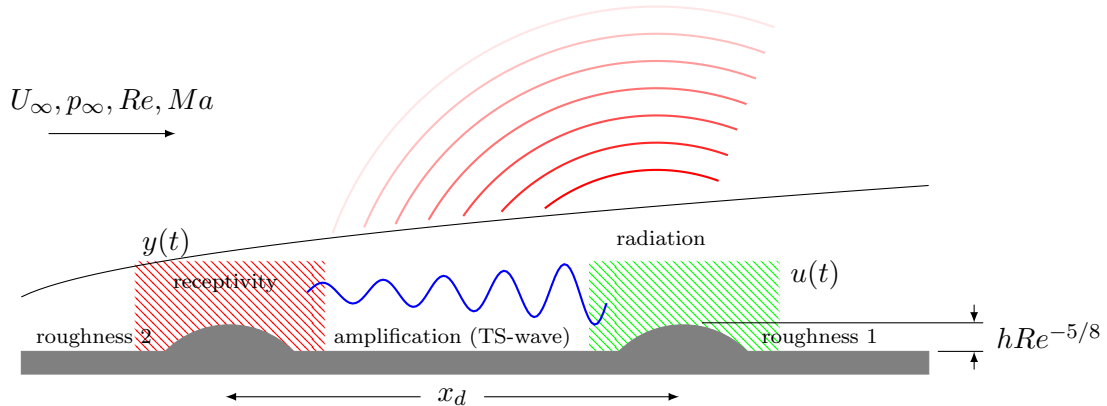
Figure 1. Sketch of the flow configuration: compressible flow over two roughness elements.

Computationally, frequency-response analyses for multiphysics flows in complex geometries require a significant effort. In many cases, we are interested in this type of analysis in a high-dimensional parameter space, describing amplification mechanisms for varying parameters, base conditions and geometries, as well as their bifurcation behavior. As a single frequency-response analysis is rather expensive, a sweep across multiple parameters is often prohibitively so.

In this study, we propose an operator perturbation approach to alleviate the cost associated with computing the parameter dependence of a frequency-response analysis [2]. We demonstrate this mathematical framework by applying it to compressible flow over a flat plate with two small roughness elements. This configuration is dominated by shear instabilities, an acoustic feedback loop and a receptivity process, all of which combine into a self-sustaining process that predominantly selects a discrete array of amplified frequencies; it is characterized by a global dynamics and thus benefits from a global analysis. Moreover, owing to the relative simplicity of this configuration, asymptotic results are readily available for validating our approach.

The analysis is based on the use of gradient and sensitivity information. This information is valuable in itself for the identification of particular responsive regions of the flow, but can also be used for optimization, active and passive control efforts, and the quantification of uncertainty in output variables given the uncertainty in input quantities.

2. Mathematical background, governing equations, numerical details

We consider compressible flow over a flat plate with two small and localized roughness elements. Figure 1 shows a sketch of the configuration. The upstream roughness (labeled roughness 2) instigates an instability (a Tollmien-Schlichting wave) that convectively grows as it travels downstream. At the downstream roughness element (labeled roughness 1) the instability interacts with the locally modified base flow and acoustic waves are radiated, predominantly upstream. These waves interact, at the upstream roughness location, with the locally altered base-flow profile and trigger again a shear-layer instability, thus closing the loop. This loop consists of a convective shear-layer instability which is permanently regenerated (near roughness 2) by the sound waves it generates farther downstream (near roughness 1). Instabilities consisting of a feedback loops are often associated with an array of frequencies that are particularly amplified, interlaced with frequencies that show little response. The behavior is related to a phase condition for the feedback and depends on the travel time of perturbations over a complete loop (convective and acoustic path); amplified frequencies correspond to a mostly constructive interference of perturbations, while damped frequencies are associated with a mostly destructive interference.

For our study, we consider the following parameters. The Reynolds and Mach number are given as $Re = 10^6$ and $Ma = 0.3$, respectively. This choice is in accordance with the work of [10] which will provide validation of our results. For simplicity, the Prandtl number and specific heat coefficient is taken as $Pr = 1$ and $\gamma = 1.4$, respectively. We follow a non-dimensionalization based on the freestream velocity U_∞ and freestream pressure p_∞; for the spatial coordinates we use l, the distance from the leading edge of the plate to the downstream roughness, as a reference length. The Reynolds number is then based on the freestream velocity and the distance from the leading edge. The roughness height distribution $f(x)$ is given as (again, following [10])

$$f(x) = hRe^{-5/8} \left[F \left(Re^{3/8}(x-1) \right) + F \left(Re^{3/8}(x-1+x_d) \right) \right] \tag{1}$$

with $F(x) = \exp(-x^2)$ and $h = 5$.

We solve the compressible Navier-Stokes equations numerically by discretizing them on a curvilinear, structured grid. We use a pseudo-characteristic formulation [8] based on the pressure, velocities and entropy. The advective terms are treated by a 5th-order compact-upwind scheme with low dissipation (CULD) [1]; a 3rd-order centered compact scheme is used for the diffusive terms. Time-stepping is performed with a 4th-order explicit Runge-Kutta scheme. Sponge layers are added to the physically relevant computational domain to enforce outflow boundary conditions and attenuate wave reflection off the computational boundaries. Details on the numerical scheme can be found in [5].

The governing equations in semi-discrete form can be written symbolically as

$$\frac{d}{dt}\mathbf{x} = \mathbf{F}(\mathbf{x}; \mu) \tag{2}$$

with $\mathbf{x}$ denoting the state vector containing all flow variables at every grid point. The variable μ represents all parameters such as $\{Re, Ma, h, x_d, \ldots\}$, i.e., related either to physical properties of the flow or geometric measurements.

The first step in our analysis consists of computing a base flow, denoted by $\mathbf{x}_0$, which solves the steady part of (2), i.e., $\mathbf{F}(\mathbf{x}_0; \mu) = 0$. We then proceed by considering perturbations $\mathbf{x}'$ about this base state and formulate a linearized governing equation for their motion. Since we are interested in an input-output analysis of this linearized system we introduce a driving term given below by $\mathbf{Bu}$, as well as a second equation that describes the output measurements $\mathbf{y}$ as a function of the state vector $\mathbf{x}'$. Our system in state-space form then reads

$$\frac{d}{dt}\mathbf{x}' = \mathbf{A}(\mathbf{x}_0(\mu); \mu)\mathbf{x}' + \mathbf{Bu}, \tag{3a}$$
$$\mathbf{y} = \mathbf{Cx}'. \tag{3b}$$

In the above expression the system matrix $\mathbf{A}$ contains the discretized linearized equations (Jacobian), the control matrix $\mathbf{B}$ specifies the spatial location and type of the forcing, while the measurement matrix $\mathbf{C}$ extracts the output variables from the full state vector $\mathbf{x}'$. The system matrix depends on the base flow $\mathbf{x}_0$ as well as on the set of parameters μ. The dependence on μ is two-fold: directly through the governing equations, and indirectly by influencing the base flow $\mathbf{x}_0$.

To further simplify our analysis, we assume a harmonic time-dependence of $\mathbf{u}(t)$, i.e., $\mathbf{u}(t) = \tilde{\mathbf{u}}\exp(i\omega t)$. Owing to the linear nature of our equations, the output variable $\mathbf{y}$ will respond with the same frequency, that is, $\mathbf{y}(t) = \tilde{\mathbf{y}}\exp(i\omega t)$. Under these assumptions, an explicit expression linking the input shape $\tilde{\mathbf{u}}$ to the output shape $\tilde{\mathbf{y}}$ can be given as

$$\tilde{\mathbf{y}} = \mathbf{C}(\mathbf{A}(\mathbf{x}_0(\mu); \mu) - i\omega\mathbf{I})^{-1}\mathbf{B}\tilde{\mathbf{u}} = \mathbf{R}(\mathbf{x}_0, \omega; \mu)\tilde{\mathbf{u}}. \tag{4}$$

We have tacitly assumed that the system matrix $\mathbf{A}$ is stable.

We proceed by formulating the gain of the harmonically driven, linearized system in the form

$$G_{\text{opt}}(\omega; \mu) = \max_{\mathbf{u}} \frac{\|\tilde{\mathbf{y}}\|_M}{\|\tilde{\mathbf{u}}\|_M} \tag{5}$$

which defines the optimal frequency response as the ratio of the energy-based output norm to the energy-based input norm, optimized over all possible input shapes $\tilde{\mathbf{u}}$. The specific energy to measure the disturbance size is Chu's energy measure for compressible flows (see Chu (1965) and Hanifi *et al.* (1996), [3],[7]). We define a scalar product and norm as follows

$$\langle \mathbf{f}, \mathbf{g} \rangle_M = \mathbf{f}^H \mathbf{M} \mathbf{g} \qquad\qquad \|\mathbf{f}\|_M^2 \equiv \langle \mathbf{f}, \mathbf{f} \rangle_M \tag{6}$$

with $\mathbf{M}$ as a positive definite matrix containing the weight factors of the energy measure as well as the integration weights over the computational domain.

The solution to the optimization problem defined by equations (5) and (4) is easily obtained by the singular value decomposition. With

$$\mathbf{M}^{1/2} \mathbf{R}(\mathbf{x}_0(\mu), \omega; \mu) \mathbf{M}^{-1/2} = \mathbf{U} \mathbf{\Sigma} \mathbf{V}^H \tag{7}$$

we can determine the components of the optimal solution as

$$\begin{array}{lll} \text{optimal forcing:} & \mathbf{u}_{\text{opt}} = \mathbf{M}^{-1/2} \mathbf{v}_1 & \\ \text{optimal response:} & \mathbf{y}_{\text{opt}} = \mathbf{M}^{-1/2} \mathbf{u}_1 & \\ \text{optimal amplification:} & G_{\text{opt}} = \sigma_1 & \end{array} \tag{8}$$

where $\mathbf{u}_1$ and $\mathbf{v}_1$ stand for the principal vector (first column) of $\mathbf{U}$ and $\mathbf{V}$, respectively, and σ_1 represents the maximum singular value (i.e., the $\mathbf{M}$-norm of $\mathbf{R}$). In practice, the calculation of the principal singular value and vectors is performed by an iterative Krylov technique, based on the matrix-free evaluation of the two matrix-vector products $\mathbf{A}\mathbf{q}$ and $\mathbf{A}^H \mathbf{q}$ for a given vector $\mathbf{q}$. Techniques for efficiently extracting the above matrix-vector products directly from nonlinear simulation codes is given in [6].

3. Analysis of the acoustic feedback loop

We will proceed by establishing the frequency response for the reference parameters given above. Before doing so, we have to decide on the regions of interest for the forcing (matrix $\mathbf{B}$) and the response (matrix $\mathbf{C}$); see also the cross-hatched areas in Figure 1. In our case, we will allow forcing in the full computational domain, but restrict the response to the half-space given by $x \leq 1.05$.

The optimal amplification to harmonic forcing is shown in Figure 2. It displays the typical characteristics of feedback-influenced globally stable flow configurations: multiple peaks at near-equispaced frequencies – with a dominant range suggesting a selection principle for a narrow frequency interval. The multiple peaks can be understood qualitatively as different realizations of a full instability-acoustics-receptivity cycle with different run times along the cyclic path. For a cycle that ends in-phase, we expect amplification and a corresponding peak at the respective frequency; for a cycle that ends out-of-phase, a trough in the frequency response is anticipated. For our parameter values, we determine the prevalent frequency range as $40 \lesssim \omega \lesssim 85$, with the peak at $\omega_p \approx 60.21$, closely matched (in optimal gain) by the second peak at $\omega_p \approx 64.55$. We also observe a nearly constant spacing of the frequency peaks with a frequency difference of $\Delta\omega_p \approx 4.3$. In a numerical simulation, as well as in a matching experiment, we thus expect to observe a low-frequency pumping at a "breathing" or beating frequency of $\omega \approx 4.3$. The exact
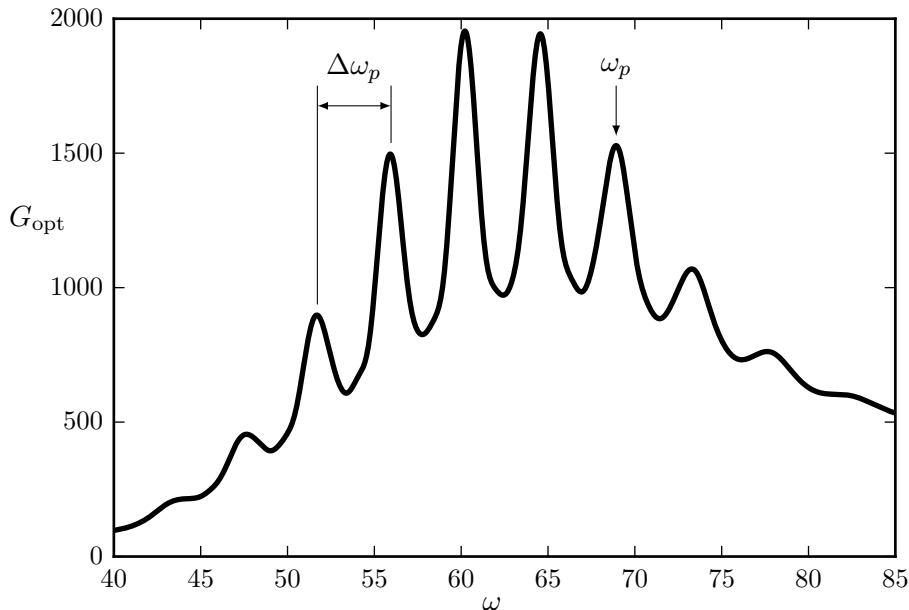
Figure 2. Frequency response for compressible flow over a flat plate with two bumps. See text for details.

Table 1. Optimal gains, peak frequencies and peak-frequency spacings.

frequency ω_p	47.64	51.70	55.92	60.21	64.55	68.92	73.28	77.61
optimal gain	454.75	898.09	1496.80	1954.48	1944.03	1528.33	1069.49	762.47
spacing $\Delta\omega_p$		4.06	4.22	4.29	4.34	4.37	4.36	4.33

values for all frequency peaks in Figure 2, the associated gain values and the frequency spacing between consecutive peaks are listed in Table 1 for reference.

As part of the optimal solution, we also recover (via the singular value decomposition) the optimal forcing and the optimal response that results in the maximum gain for a given frequency, as displayed in Figure 2. We visualize both fields by the streamwise velocity and the pressure, in order to approximately delineate the effects of convection and acoustic radiation. The results are depicted in Figure 3. Considering the streamwise velocity, we see the optimal forcing localized upstream of roughness 2 and concentrated in the boundary layer (see Figure 3a): the most sensitive region for achieving maximal amplification of forcing at a frequency of $\omega = 56$ is ahead of the upstream element. A response to this type of forcing is mostly concentrated downstream of roughness 1 and shows non-zero components in the boundary layer as well as the freestream (see Figure 3b). The physical separation of input and output suggests a convective link, with a dominant propagation of information in the downstream direction. We conclude that the advection of instabilities is certainly part of the full dynamic cycle, but is not responsible for upstream propagation.

A different picture emerges when considering the pressure part of the optimal forcing and response (see Figures 3c,d). In this case, the optimal forcing again shows non-zero contributions
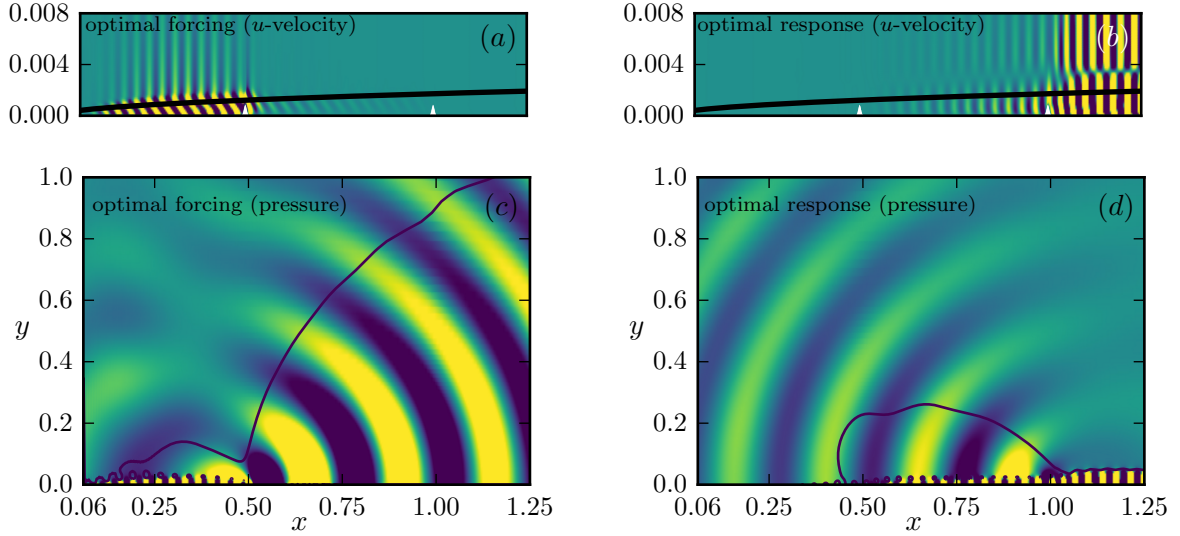
Figure 3. Optimal forcing (left) and response (right) for a forcing frequency $\omega = 60.25$, visualized by contours of the streamwise velocity (a,b) and pressure (c,d).

upstream of roughness 2, however with a significant amount of acoustic radiation pointed predominantly downstream. The response to this forcing, in contrast to the streamwise velocity component, is pointed upstream establishing a dynamic link between the downstream and upstream roughness element. In other words, the pressure-part of the optimal process forms a feedback connection between roughness 1 and 2.

The full harmonic process thus consists of a convective instability (directed mostly downstream) and an acoustic feedback (directed upstream) which, via a receptivity process, retriggers the convective instability.

4. Parametric sensitivity analysis

After having established the frequency response for our reference case, we are now interested in the question how the amplification and peak location change as the parameters of the reference configuration are altered. However, we wish to avoid repeated frequency-response calculations for varying parameters. Instead, we invoke a perturbation approach for the singular value decomposition during the frequency-response computation [2,9,4]. In order to avoid the inversion in the definition of the resolvent, we slightly reformulate the problem and perturb the smallest singular value of $\mathbf{R}^+$, the pseudo-inverse of $\mathbf{R}$, following

$$\mathbf{R}^+(\mathbf{x}_0(\mu + \delta\mu), \mu + \delta\mu; \omega) = (\mathbf{V} + \delta\mathbf{V})(\mathbf{\Sigma} + \delta\mathbf{\Sigma})^{-1}(\mathbf{U} + \delta\mathbf{U}). \tag{9}$$

Using straightforward linear-algebra manipulations, we arrive at

$$\delta\left(\frac{1}{\sigma}\right) = -\frac{\delta\sigma}{\sigma^2} = -\text{Real}\left\langle \mathbf{u}_{\text{opt}}, \frac{\partial\mathbf{R}^+}{\partial\mu}\mathbf{y}_{\text{opt}}\right\rangle \tag{10}$$

with the abbreviation

$$\frac{\partial\mathbf{R}^+}{\partial\mu} = -\mathbf{B}^T\left(\frac{\partial\mathbf{A}}{\partial\mathbf{x}_0}\frac{\partial\mathbf{x}_0}{\partial\mu} + \frac{\partial\mathbf{A}}{\partial\mu}\right)\mathbf{C}^T. \tag{11}$$

We recognize in the latter expression the parametric derivatives of $\mathbf{A}$ with respect to changes in the base flow and via its direct dependence on μ. We also notice that the matrix $\dfrac{\partial\mathbf{R}^+}{\partial\mu}$

cannot be formed explicitly; fortunately, we only need the matrix-vector product $\dfrac{\partial \mathbf{R}^+}{\partial \mu}\mathbf{y}$. We thus approximate the matrix-vector product by a finite-difference scheme according to

$$\frac{\partial \mathbf{R}^+}{\partial \mu}\mathbf{y} \approx \frac{\mathbf{B}^T \mathbf{A}(\mathbf{x}_0(\mu + \epsilon\mathbf{e}_k), \mu + \epsilon\mathbf{e}_k)\mathbf{C}^T\mathbf{y} - \mathbf{B}^T \mathbf{A}(\mathbf{x}_0(\mu), \mu)\mathbf{C}^T\mathbf{y}}{\epsilon} \qquad (12)$$

and choose $\epsilon = \{10^{-1}, 10^{-2}, 10^{-3}, 10^{-4}\}$.

4.1. Sensitivity with respect to Reynolds number

We commence by probing the sensitivity of the frequency response with respect to the Reynolds number. Applying the gradient formula above, we obtain the sensitivity curve shown in figure 4a. In this plot, we indicate the peak frequencies by vertical gray lines. We observe that the sensitivity measure $\partial G_{\mathrm{opt}}/\partial Re$ nearly aligns with the frequency peaks. All gradients are positive, demonstrating that an increase in Reynolds number above the reference value will result in an increase in the frequency response across all frequencies displayed in Figure 4a; in other words, the flow destabilizes for higher Reynolds numbers. Near the peak frequencies (gray lines) we observe a proportionally higher sensitivity, and thus a higher absolute change in G_{opt} at the peak frequencies.

In figure 4b, we display the changes in the streamwise component of the base flow as the Reynolds number is changed. We see that increasing the Reynolds number has a mostly favorable effect on base flow, except for the recirculation region of both roughness elements, where the parametric gradient is negative. We recall that this gradient field is a component of the overall frequency-response sensitivity, denoted by $\partial \mathbf{x}_0/\partial \mu$ in (11).

4.2. Sensitivity with respect to Mach number

A different behavior can be observed when assessing the sensitivity of the frequency response to changes in the Mach number. Figure 5a displays the gradient of G_{opt} with respect to Ma for the frequencies in Figure 2. Again, we mark the unperturbed peak frequencies by vertical gray lines. In contrast to the previous example, we observe positive and negative gradients. In fact, left of the peak frequency a positive gradient is observed, while right of it the gradient is negative. The combined action produces a shift of the peak frequency to lower values as the Mach number is increased from the reference value of $Ma = 0.3$. This effect accounts for the reduced travel time along the acoustic feedback loop and a correspondingly modified phase condition for optimal amplification.

Figure 5b shows the gradient of the streamwise base-flow component with respect to the Mach number. Nonzero gradients are observed near both roughness elements, with strong negative values in their immediate wakes. The majority of positive changes (with an increase in the Mach number) is concentrated at the roughness location and shows influences both in the boundary layer and the freestream.

4.3. Sensitivity with respect to roughness height

After having analyzed the sensitivity with respect to physical parameters, we now proceed to consider changes in the geometry, namely the height h of the roughness elements. Figure 6a shows positive gradients, indicating that an increase in the roughness height intensifies the gain G_{opt} across all considered frequencies, thus yielding a less stable flow configuration. In this respect, an increase in roughness height has a qualitatively similar effect on the frequency response as an increase in the Reynolds number (for which also only positive gradients have been found).
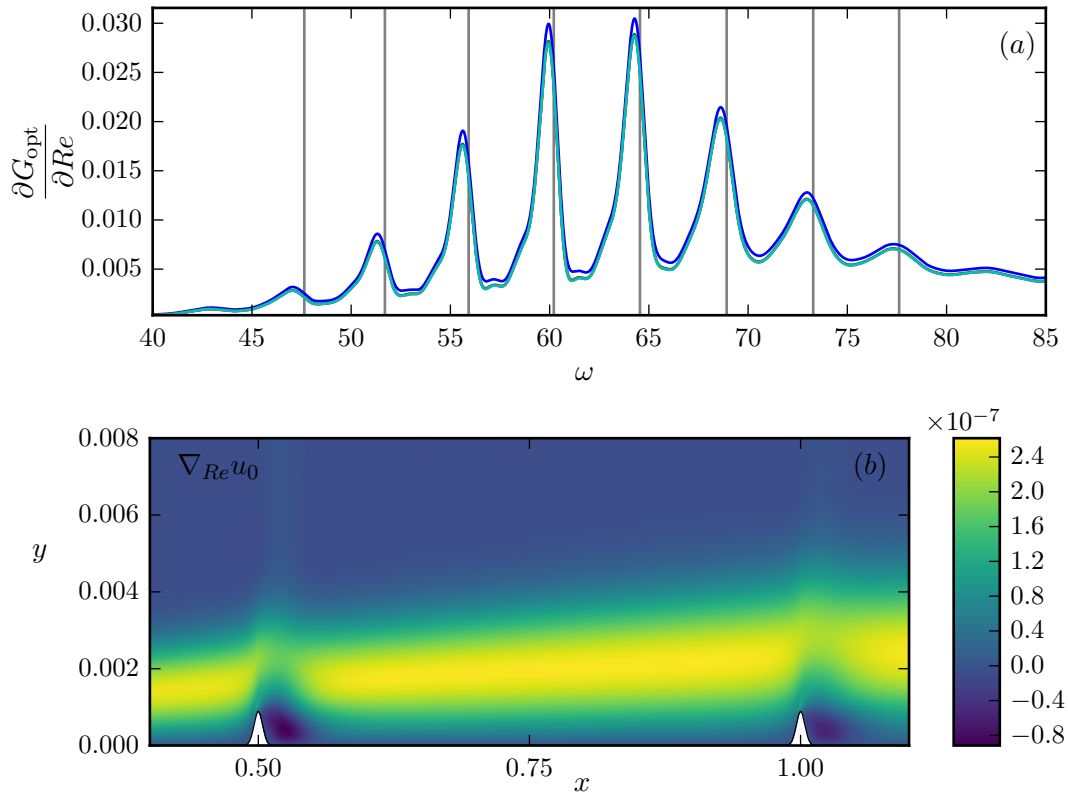
Figure 4. Sensitivity of the frequency response with respect to Reynolds number. (a) Gradient of the optimal gain with respect to Reynolds number. (b) Gradient of the base flow with respect to the Reynolds number. The various curves represent the frequency response from (12) for values of the parameter ϵ in $\{10^{-1}, 10^{-2}, 10^{-3}, 10^{-4}\}$ (blue to green).

The change in the base flow, as the roughness height is increased, shown in Figure 6b, is however distinctly different from the Reynolds number gradient field. It shows far stronger localization at and in the wake of the roughness elements.

4.4. Sensitivity with respect to roughness separation
Finally, we quantify the parametric sensitivity with respect to changes in the separation of the two roughness elements. The gradient with respect to h_L is shown in Figure 7a. As before for the case of Mach-number-sensitivity, we notice alternating signs for the gradient. With positive gradients at frequencies slightly lower than the peak values, and negative gradients at frequencies slightly above, we can deduce a down-shift in peak frequencies as the separation distance increases. Qualitatively, this is similar to an increase in Mach number. With the run-time of acoustic waves between emission point (roughness 1) and receptivity point (roughness 2) as the critical variable for in-phase amplification, we see that the speed of wave propagation (related to the Mach number) and the travel distance (related to the roughness separation) have similar qualitative effects and thus similar frequency-response gradients.

Figure 7b displays the gradient field of u_0 (the streamwise component of the base flow) with respect to the roughness separation x_d. The gradient obviously concentrates on roughness 1, since roughness 2 is left unchanged. We see a typical positive-negative gradient contour centered on the element, describing changes in the base-flow profile by displacing the roughness element
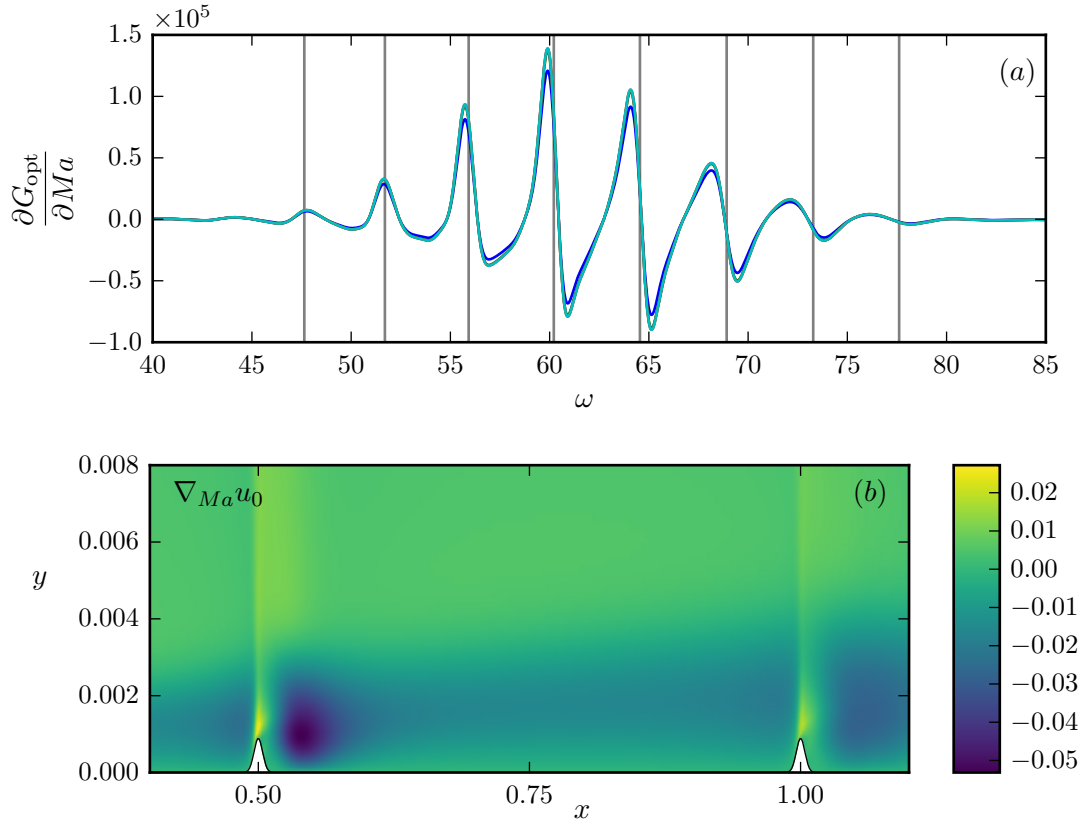
Figure 5. Sensitivity of the frequency response with respect to Mach number. (a) Gradient of the optimal gain with respect to Mach number. (b) Gradient of the base flow with respect to the Mach number. The various curves represent the frequency response from (12) for values of the parameter ϵ in $\{10^{-1}, 10^{-2}, 10^{-3}, 10^{-4}\}$ (blue to green).

farther upstream.

4.5. Validation of sensitivity information

The sensitivity measures for the frequency response gain, obtained from the use of adjoint information via an appropriately weighted scalar product, can be validated by a simple (but costly) calculation of frequency response data for slightly modified parameters, followed by a repeated singular value decomposition. This procedure has been undertaken for small changes in our four parameters: the Reynolds number Re, the Mach number Ma, the roughness height h_L, and the roughness separation length x_d. In all cases, a relative change of 10^{-4} has been chosen; while the sensitivity measures are expected to give reasonable approximations beyond this small perturbation in the parameters, the small relative change will aid in gaining confidence and assessing validity of the introduced sensitivity formula. In addition, due to the appreciable computational effort, we restrict ourselves to an annular-frequency band of $57.5 \leq \omega \leq 62.5$, where some of the most prominent sensitivity peaks have been encountered.

Figure 8 compares the sensitivity measures obtained from gradient information (indicated by solid lines) to sensitivity measures calculated by repeated singular value decompositions of frequency response calculations (displayed by symbols). For each of the four parameter variations, we see good agreement between the two methods. The sensitivities capture the type, amplitude and frequency peak very well: for the sensitivities with respect to the Reynolds
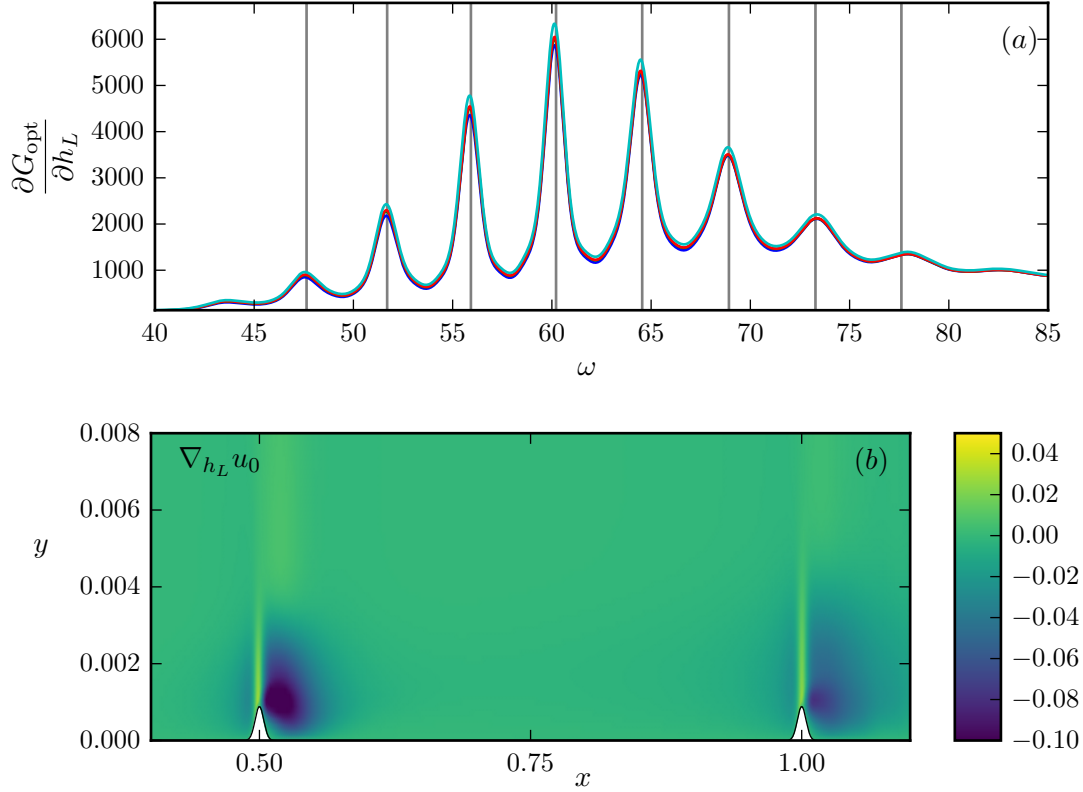
Figure 6. Sensitivity of the frequency response with respect to roughness height. (a) Gradient of the optimal gain with respect to roughness height. (b) Gradient of the base flow with respect to the roughness height. The various curves represent the frequency response from (12) for values of the parameter ϵ in $\{10^{-1}, 10^{-2}, 10^{-3}, 10^{-4}\}$ (blue to green).

number and roughness height, a single peak is observed in both cases that suggests a dominant influence on the gain but a negligible gain on the frequency to first order; for the sensitivities with respect to the Mach number and roughness separation length, a shift in the most amplified frequency can be implied, in both cases towards lower frequencies for a positive change in the Mach number or roughness separation length. This comparison lends credibility to the far simpler sensitivity calculation by weighted scalar products of direct and adjoint structures.

5. Conclusions

Globally stable flow configurations that act as selective amplifiers of environmental noise and uncertainties can effectively be described and analyzed by their frequency response to harmonic excitation. This type of analysis is particularly appropriate when a feedback between downstream propagating instabilities and upstream receptivity is present. This configuration was demonstrated in this article by a compressible boundary layer flow perturbed by two localized and separated wall protrusions. Tollmien-Schlichting (TS) instabilitiy waves are generated at the upstream roughness which induce acoustic waves at the downstream protrusion. The acoustic waves travel predominantly upstream and regenerate TS-waves at the first bump, thus closing the feedback loop.

The frequency-response analysis of this configuration showed a typical multi-peak behavior with preferred near-double peak frequencies at $\omega \approx 60$ and $\omega \approx 64.5$. The corresponding forcing
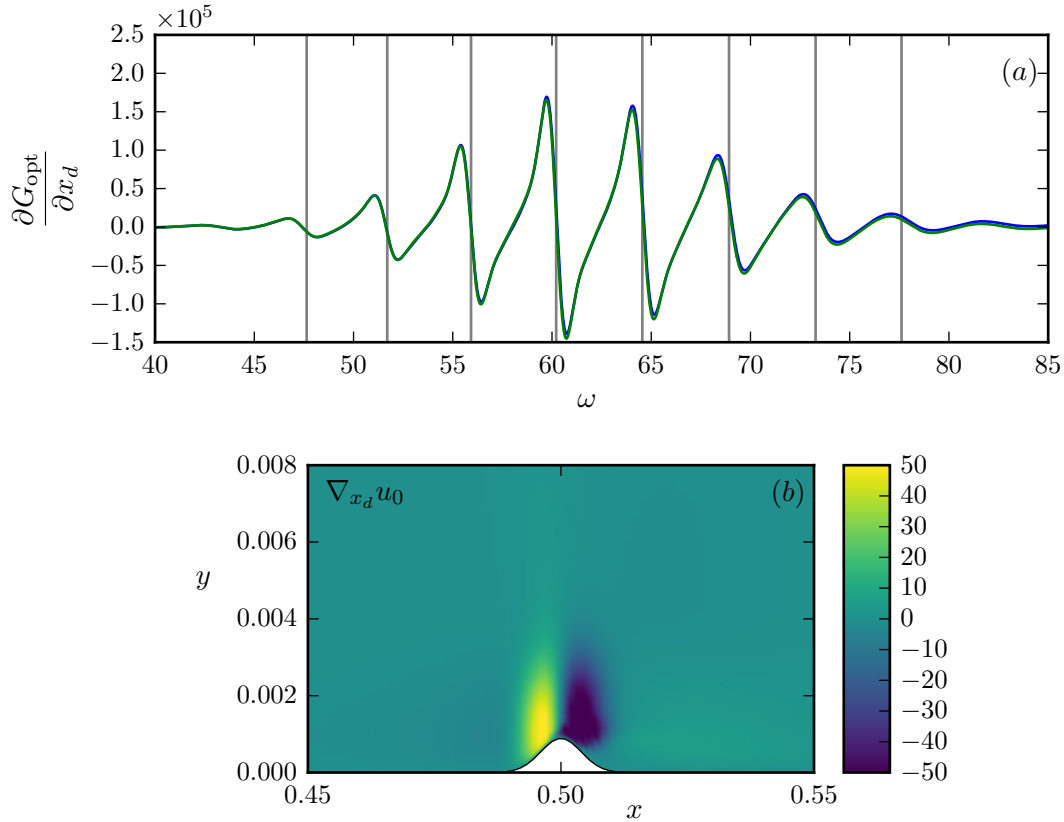
Figure 7. Sensitivity of the frequency response with respect to roughness separation. (a) Gradient of the optimal gain with respect to roughness separation. (b) Gradient of the base flow with respect to the roughness separation. The various curves represent the frequency response from (12) for values of the parameter ϵ in $\{10^{-3}, 10^{-4}\}$ (blue to green).

and response fields confirm the decomposition of the full (global) instability characteristics into a downstream-convective part and an upstream-propagating acoustic component. A comparison between the adjoint-based sensitivities and the (far more inefficient) solution of the optimization problem showed a good match, corroborating the accuracy of our approach.

A parametric sensitivity formalism of the frequency response with respect to the governing parameters (both physical and geometric) has been introduced and applied to forcing at a frequency of $\omega = 56$, a side-peak in the frequency response. The gradients with respect to Reynolds number or roughness height were found to be positive for all considered frequencies, indicating that an increase in either of these parameters causes a destabilization of the flow. The gradients with respect to Mach number and roughness separation shows both positive and negative values as the frequency is varied. The gradient curves are such that an increase in Mach number or roughness separation brings about a shift in the frequency peaks towards lower frequencies. This feature can be explained as follows: both increasing the Mach number or the roughness separation result in a change in the acoustic travel time from the scattering point (roughness 1) to the receptivity point (roughness 2); the necessary adjustment in frequency to comply to a constructive interference (phase condition) to produce a peak in the frequency response entails a shift to lower frequencies.

It is important to keep in mind that the parametric sensitivity analysis – and the information it furnsihed – did not require additional (costly) computations of frequency responses. This
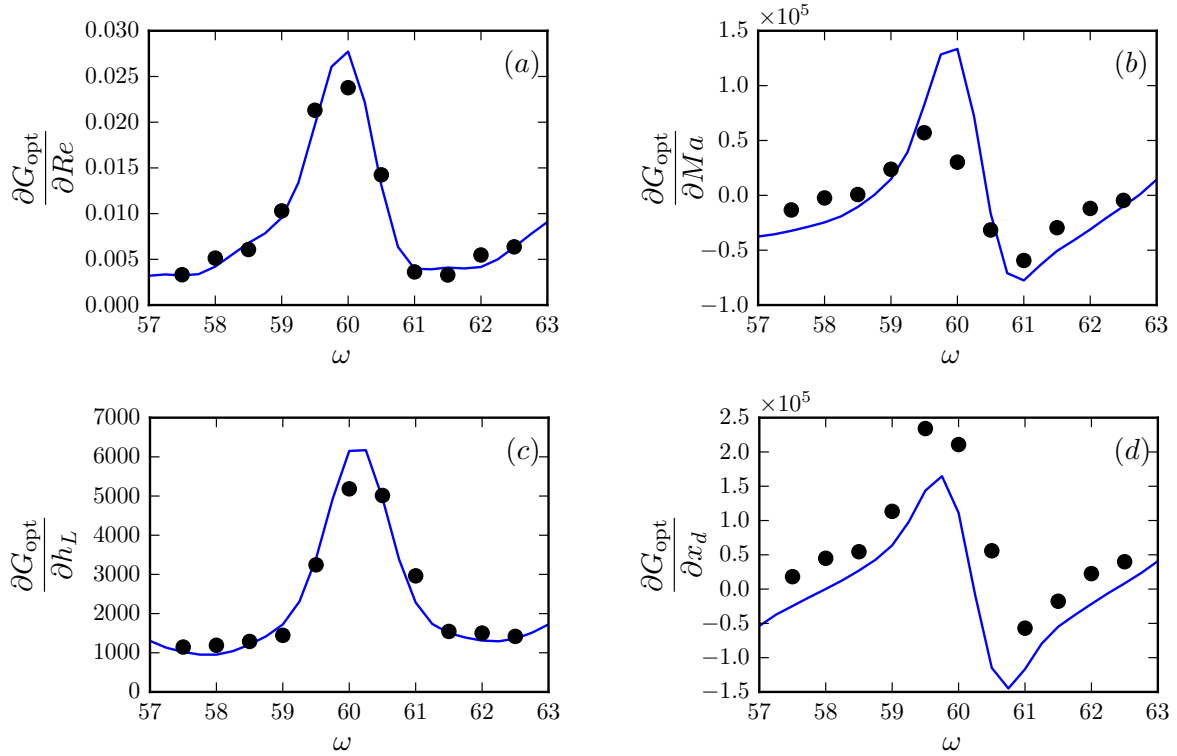
Figure 8. Sensitivity of the frequency response with respect to four parameters: (a) Reynolds number, (b) Mach number, (c) roughness height, and (d) roughness separation length. In each subplot, the solid line refers to the optimal-gain sensitivity using gradient information; the sensitivity using multiple optimal-gain calculations for a 10^{-4} relative increase in these parameters is indicated by black symbols.

information has been acquired purely by efficient matrix multiplications of quantities already available from the reference case. As such, this type of investigation provides great insight into fluid flows that are driven by a complex interplay of multiple competing physical mechanisms, including the dominance of any of these mechanisms as physical parameters are changed or geometries are modified. Moreover, this insight is gained at a negligible computational cost. We anticipate further and interesting applications of parametric sensitivity analysis to aeroacoustic and thermoacoustic flow configurations, with implications on the analysis, control and design improvement of the associated fluid devices.

Acknowledgments

[1] Adams, N.A. and Shariff, K. 1996 A high-resolution hybrid compact-ENO scheme for shock-turbulence interaction problems. *J. Comp. Phys.* **127**(1), pp. 27–51.

[2] Brandt, L., Sipp, D., Pralits, J. and Marquet, O. 2011 Effect of base-flow variation in noise amplifiers: the flat-plate boundary layer. *J. Fluid Mech.* **687**, pp. 503–528.

[3] Chu, B.-T. 1965 On the energy transfer to small disturbances in fluid flow. *Acta Mech.* **1**(3), pp. 215–234.

[4] Fosas de Pando, M., Schmid, P.J. and Lele, S. 2014 Parametric sensitivity for large-scale aeroacoustic flows. *Proc. CTR Summer Prog.*, pp. 365–374.

[5] Fosas de Pando, M., Schmid, P.J. and Sipp, D. 2014 A global analysis of tonal noise in flows around aerofoils. *J. Fluid Mech.* **754**, pp. 5–38.

[6] Fosas de Pando, M., Sipp, D. and Schmid, P.J. 2012 Efficient evaluation of the direct and adjoint linearized dynamics from compressible flow solvers. *J. Comput. Phys.* **231**, pp. 7739-7755.

[7] Hanifi, A., Schmid, P.J. and Henningson, D.S. 1996 Transient growth in compressible boundary layer flow. *Phys. Fluids* **8**(3), pp. 826–827.

[8] Sesterhenn, J. 2001 A characteristic-type formulation of the Navier-Stokes equations for high order upwind schemes. *Comp. Fluids* **30**(1), 37–67.

[9] Sipp, D. and Marquet, O. 2013 Characterization of noise amplifiers with global singular modes: the case of the leading-edge flat-plate boundary layer. *Theor. Comp. Fluid Dyn.* **27**(5), 617–635.

[10] Wu, X. 2011 On generation of sound in wall-bounded shear flows: back action of sound and global acoustic coupling. *J. Fluid Mech.* **689**, pp. 279–316.